A Numerical Study on the Effects of Initial Water Saturation of a Geothermal Reservoir on Well Characteristics

Khasani
Department of Earth Resources Engineering : Graduate Student

Itoi, Ryuichi
Department of Earth Resources Engineering : Professor

Tanaka, Toshiaki
Department of Earth Resources Engineering : Research Associate

Fukuda, Michihiro
Department of Earth Resources Engineering : Professor Emeritus

出版情報：九州大学工学紀要. 64 (1), pp.1-15, 2004-03. 九州大学大学院工学研究院
バージョン：
権利関係：

Memoirs of the Faculty of Engineering, Kyushu University, Vol. 64, No. 1, March 2004

A Numerical Study on the Effects of Initial Water Saturation of a Geothermal Reservoir on Well Characteristics

by

KHASANI*, Ryuichi ITOI**, Toshiaki TANAKA***
and Michihiro FUKUDA****

(Received December 10, 2003)

Abstract

The effects of initial water saturation on well characteristics in two-phase geothermal reservoirs were evaluated. A vertical wellbore model of uniform diameter coupled with a radial horizontal flow in a reservoir of uniform thickness was employed. The momentum equation for two-phase flow in a wellbore was numerically evaluated with a method introduced by Orkiszewski. The energy equation in the wellbore was assumed to be isenthalpic. Mass flow rate and pressure at a feed zone of the well were calculated using a steady radial flow in a reservoir. The numerical calculation showed that the lower initial water saturation in the two-phase reservoir leads to less total flow rate at a given wellhead pressure. However, the decrease in the initial water saturation results in an increase in the maximum discharge pressure. The initial water saturation does not affect the steam flow rate significantly for low wellhead pressure.

Keywords: Two-phase reservoir, Water saturation, Well characteristics, Wellbore flow

1. Introduction

In the course of geothermal development for power generation, understanding of well performances and evaluation of well deliverability are important tasks for reservoir management. This is because predicting steam discharge rate from wells and evaluating the effects of reservoir conditions on the steam flow rate provide valuable information for designing the size of a power plant. As the production stage of a field begins, stable production of steam from wells is often impeded by problems such as declines of reservoir pressure and tempera-

* Graduate Student, Department of Earth Resources Engineering
** Professor, Department of Earth Resources Engineering
*** Research Associate, Department of Earth Resources Engineering
**** Professor Emeritus, Department of Earth Resources Engineering

ture.

Wellbore simulators are powerful tools for evaluating well performances such as pressure and temperature distributions in a well and well deliverability. They solve a set of mathematical equations that describe two-phase flows of steam and water mixture in a wellbore. Thus, the simulators can be used for evaluating the effects of well parameters such as diameter and depth on well performances. Furthermore, since reservoir conditions give effects on well performances, reservoir fluid flow in the vicinity of wells should be included in the wellbore simulator for providing reliable results.

There are several papers that discuss and review existing wellbore simulators. Bjornsson and Bodvarsson developed a multi-feedzone wellbore simulator that allows for calculations of downhole pressure, temperature and quality in wells with an arbitrary number of feed zones[1]. It can simulate fluid properties in a well during both discharge and injection and evaluate internal flow and relative contributions of feedzones. Another multipurpose wellbore simulator was developed by Hadgu and Freeston[2]. The simulator can handle the flow with dissolved solids and gases and allow multifeed well simulation when adequate information on feed zones is available. It also includes heat loss and different geometry of wells with different pipe roughness. However, these two simulators do not include reservoir flows in their model. Takahashi developed a wellbore simulator that was coupled with a reservoir flow. It can handle single and two-phase flows in the reservoir[3]. He does not, however, consider distributions of density and viscosity of two-phase fluids in the vicinity of well. Hadgu *et al.* described the wellbore simulator (WFSA) coupled with reservoir simulator (TOUGH)[4]. The coupled simulator is capable, for example, of determining pressure and mass flow rate versus time and evaluating power output scenarios. The model of Hadgu *et al.* can handle both initially the single and the two-phase conditions in the reservoir. The above two simulators presented the samples of deliverability curves as a tool for evaluating well performances.

One of the purposes of wellbore simulation is to evaluate well performances expressed by its deliverability curve as discussed by several papers: Gudmundsson[5], Brennand and Watson[6], Garg *et al.*[7] and Gutierrez *et al.*[8]. The last paper included a reservoir model and a discussion on computed deliverability curve to evaluate the well characteristics and pressure profiles in wellbore. The main feature of the model is its use of two-phase homogeneous flow model in wellbore. A typical deliverability curve obtained from field measurements of Well S-4 at the Sumikawa geothermal field in Japan was presented by Garg[9]. A similar curve was observed on Well 703 at Rotorua, New Zealand (Brennand and Watson)[6]. The obtained deliverability curves from measurements were fairly similar to those produced by the above wellbore simulators.

The study of two-phase reservoirs is important because reservoirs of high temperature initially single liquid phase easily evolve to two-phase conditions as reservoir pressure declines with development. The wellbore models above can be divided into two groups: models including and not including reservoir flow. Although the model including reservoir flow can handle two-phase conditions in reservoir, the effects of water saturation of reservoir on well characteristics have not been discussed in detail. This paper, therefore, deals with the effects of initial water saturation in the two-phase reservoir on well characteristics using a wellbore model that includes a steady radial flow in a reservoir.

2. Governing Equations

The governing equations are for wellbore equations that are coupled with the fluid flow

in a reservoir. The schematic diagram of the reservoir and wellbore model is illustrated in **Fig. 1**.

2.1 Equations for reservoir

Basic equations for fluid flow in the reservoir are derived under assumptions as follow (Itoi *et al.*)[10]:

1) reservoir is of radial symmetry and horizontal with a constant thickness
2) fluid flow obeys Darcy's law and is under steady state
3) no heat exchange between fluid and reservoir rock and the flow follows isenthalpic process.

Continuity equations of mass and momentum in the reservoir are expressed as:

$$-\frac{1}{r}\frac{\partial(ru)}{\partial r}=0 \tag{1}$$

$$u=\frac{k}{\nu_t}\frac{\partial p}{\partial r} \tag{2}$$

where r is the radial distance (m), u is the mass flux density (kg/m^{2}s), k is the permeability (m^2), ν_t is the total kinematic viscosity of two-phase fluid (m^2/s) and p is the pressure (Pa). Mass flux density is the sum of steam and water flux densities (u_s and u_w) and written as

$$u=u_w+u_s$$
$$=-\left(\frac{kk_{rw}}{\nu_w}+\frac{kk_{rs}}{\nu_s}\right)\frac{\partial p}{\partial r} \tag{3}$$

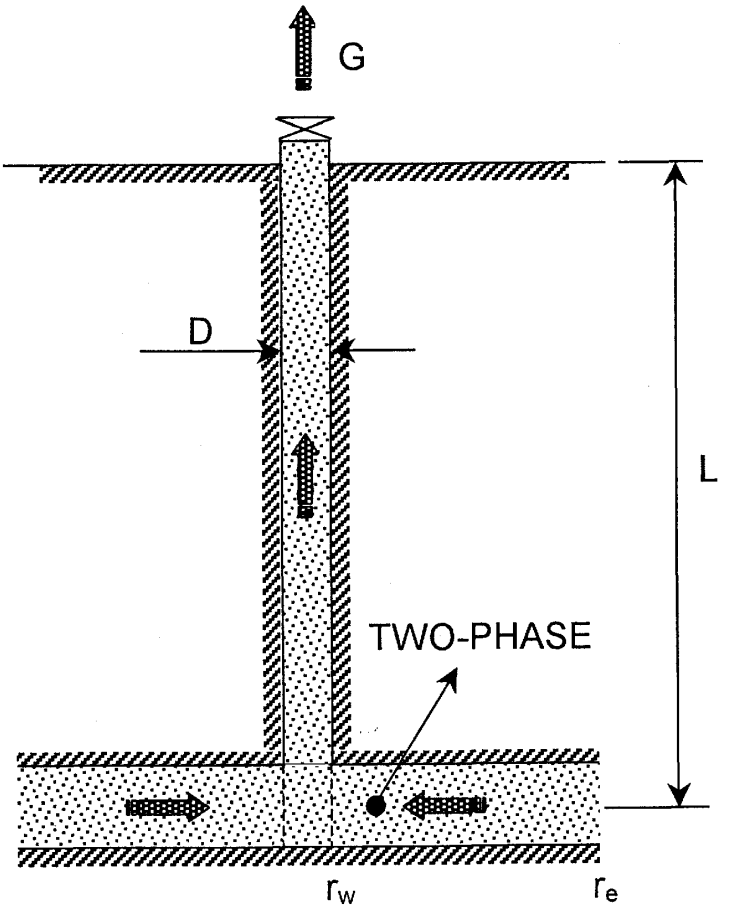

Fig. 1 Schematic diagram of reservoir-wellbore model.

Here k_{rw} and k_{rs} are the relative permeability to water and steam (-), respectively, ν_w and ν_s are the kinematic viscosity of water and steam (m^2/s), respectively.
Then, the total kinematic viscosity, ν_t, can be defined as (Grant *et al.*)[11]:

$$\frac{1}{\nu_t}=\frac{k_{rw}}{\nu_w}+\frac{k_{rs}}{\nu_s} \tag{4}$$

From the definition of two-phase fluid enthalpy (Grant *et al.*)[11], relative permeabilities can be expressed using enthalpies of steam and water:

$$\frac{k_{rs}}{k_{rw}}=\frac{\nu_s(i_w-i)}{\nu_w(i-i_s)} \tag{5}$$

where i is the total enthalpy of fluid (J/kg), i_w is the enthalpy of water (J/kg) and i_s is the enthalpy of steam (J/kg).

Relative permeabilities can be expressed as a function of water saturation in porous media or fractured media. In this study, the correlation between relative permeabilities is expressed in an X-curve that satisfies the following expression:

$$k_{rs}+k_{rw}=1 \tag{6}$$

then, ν_t can be expressed as:

$$\frac{1}{\nu_t}=\frac{(i_w-i_s)}{\nu_w(i-i_s)+\nu_s(i_w-i)} \tag{7}$$

Flow rate of the two-phase mixture entering the wellbore at the feed zone can be calculated by:

$$G=-uA|_{r_w}=2\pi r_w h\left(\frac{k}{\nu_t}\frac{\partial p}{\partial r}\right)_{r_w} \tag{8}$$

with boundary conditions written as:

$$r=r_w \ : \ p=p_{wb}$$
$$r=r_e \ : \ p=p_e$$

where r_w is the wellbore radius (m), h is the thickness of reservoir (m), A is the surface area of the feed zone (m^2). Subscript e denotes the outer boundary of reservoir. The pressure gradient at $r=r_w$ in Eq. (8) is calculated from the solution of Eq. (1) under the boundary conditions above. Because the total kinematic viscosity in Eq. (8) is a function of either pressure or temperature under saturated conditions, Eq. (8) is expressed in the integral form as

$$G=2\pi kh\frac{\int_{p_{wb}}^{p_e}\frac{\partial p}{\nu_t}}{R_e} \tag{9}$$

where R_e is the normalized distance of $r_e(R_e=\ln(r_e/r_w))$. The integral part in Eq. (9) is numerically evaluated with Simpson's method.

2.2 Wellbore model

The basic equations for two-phase flow in the wellbore are derived under assumptions as follow:

1) the fluid flows into the well from a single feed zone at well bottom
2) the well is vertical with uniform diameter

3) the fluid flow in the well is under steady state and isenthalpy

The basic equations used for two-phase flow in the wellbore consist of conservation of mass and momentum as follow:

$$\frac{dM}{d\ell}=0 \tag{10}$$

$$\Delta P_t-\{\Delta P_a+\Delta P_h+\Delta P_f\}=0 \tag{11}$$

where M is the total mass flow rate (kg/s), ℓ is the depth coordinate (m), ΔP_t is the total pressure drop (Pa), ΔP_a is the pressure drop due to acceleration (Pa), ΔP_h is the pressure drop due to potential (Pa) and ΔP_f is the pressure drop due to friction (Pa).

2.3 Pressure losses evaluation

The classification of flow regimes for two-phase flow proposed by Orkiszewski[12], as bubble, slug, transition and mist, is used for evaluating pressure losses. Each regime has its own formula for calculating void ratio. Using this void ratio, the mixture density can be determined. All pressure drop components require the mixture density to calculate their values.

1) Pressure drop due to potential (ΔP_h)

Potential loss for vertical two-phase flow in a small length increment ΔL (m) is given as

$$\Delta P_h=\rho_m\cdot g\cdot\Delta L \tag{12}$$

$$\rho_m=\alpha\rho_g+(1-\alpha)\rho_l \tag{13}$$

where ρ_m is the mixture density (kg/m^3) and g is the gravitational acceleration (m/s^2). α is the void ratio (-) that is determined using the method by Orkiszewski.

2) Pressure drop due to acceleration (ΔP_a)

Acceleration loss for the two-phase flow with the specific volume (ν_m) between two adjacent elements at points below and above of the length increment ΔL, indicated by subscript 1 and 2 respectively, then

$$\Delta P_a=\left(\frac{M}{F}\right)^2(\nu_{m,1}-\nu_{m,2}) \tag{14}$$

where F is the cross sectional area of the well (m^2).

3) Pressure drop due to friction (ΔP_f)

Friction loss is calculated using the following equation

$$\Delta P_f=\frac{\lambda_m}{2D}\frac{M^2}{\rho_m A^2}\Delta L \tag{15}$$

where D is the well diameter (m). λ_m is the friction factor for two-phase flow (-) and evaluated using the equations proposed by Swamee & Jain:

$$\lambda_m=\frac{0.25}{\left[\log\left(\frac{\varepsilon/D}{3.7}+\frac{5.74}{Re^{0.9}}\right)\right]^2} \tag{16}$$

where ε is the pipe roughness (m) and Re is Reynolds number (-). Re is calculated for two-phase flow fluids where average kinematic viscosity and velocity are evaluated for respective flow regimes.

3. Calculation procedures

3.1 Input parameters for calculation

The parameters for reservoir and wellbore used in this study are summarized in **Table 1**. The reservoir temperature is given to be 280°C. The corresponding saturation pressure is 64 bar. To evaluate the effects of permeability thickness (*kh*) on well characteristics, two values are used, i.e. 3×10^{-12}m^3 (3 darcy-m) and 5×10^{-12}m^3 (5 darcy-m). The initial water saturation (*Swi*) is given as 0.5 and 0.1. The roughness of the inner surface of the wellbore is taken as that of commercial steel pipe.

3.2 Calculation procedure

The first step of calculation is to read input data for both reservoir and wellbore. Then, the feed zone pressure, *Pwb*, is calculated using Eq. (9) under a specified mass flow rate. As *Pwb* is implicitly expressed in the integration term of Eq. (9), the bi-section method was adopted to find the value of *Pwb* that satisfies Eq. (9). The obtained *Pwb* together with the mass flow rate are used as input data for wellbore calculation.

The wellbore calculation basically computes the total pressure drop in the wellbore that depends on the flow regimes. A small pressure increment ΔP (0.5 bar) is given, and a corresponding length increment ΔL is calculated. This procedure starts from the feed zone at pressure *Pwb*, and is repeated until the summation of ΔL reaches to the total length of well. Then, wellhead pressure, P_{WH}, is obtained. Fluid thermodynamic properties are calculated with PROPATH[14] and are evaluated for average values using pressures at both ends of the segment. Then, the pressure, enthalpy and dryness fraction at the wellhead are finally attained.

Table 1 Reservoir and wellbore parameters.

	Parameter	Value
Reservoir	Temperature (T)	280 (^{0}C)
	Pressure (P)	64 (bar)
	Horizontal Extent (r_e)	50 (m)
	Permeability Thickness (kh)	3×10^{-12} , 5×10^{-12} (m^3)
	Initial Water Saturation (Swi)	0.5, 0.1 (-)
Wellbore	Diameter (D)	0.2 (m)
	Length (L)	1000 (m)
	Roughness (ε)	4.6×10^{-5} (m)

4. Results and Discussion

4.1 Deliverability curves for different permeability thickness (kh)

Figure 2 shows deliverability curves for different permeability thickness, *kh*, with parameters of initial water saturation of reservoir, *Swi*. Two cases of permeability thickness, 3 darcy-m and 5 darcy-m, are considered. *Swi* are given to be 0.1 and 0.5. Deliverability curves represent the relationship between mass flow rate and wellhead pressure, which can be used to evaluate well productivity as well as well characteristics.

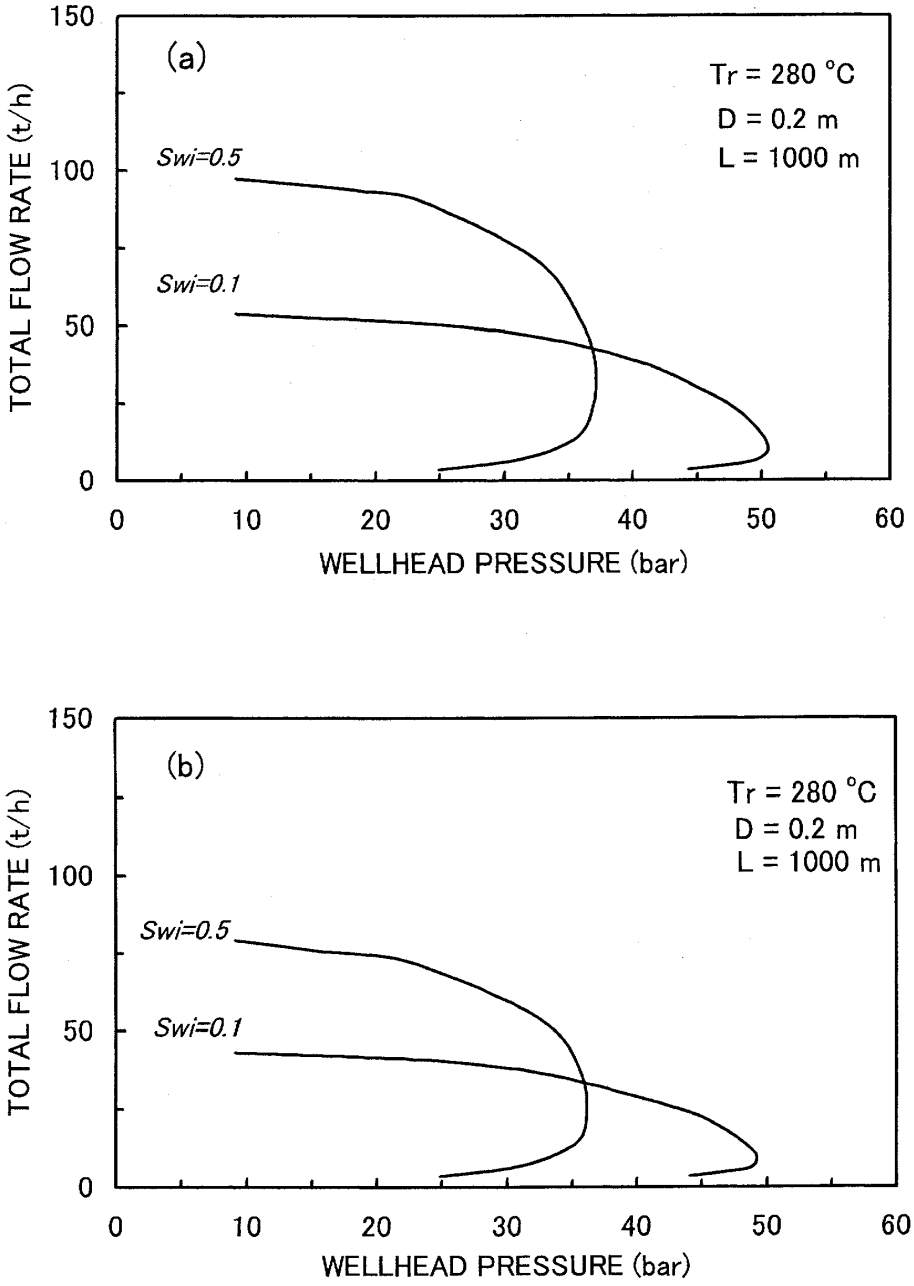

Fig. 2 Effects of initial water saturation in reservoir (*Swi*) on deliverability curves: (a) *kh*=5 darcy-m, (b) *kh*=3 darcy-m.

As shown in **Fig. 2(a)** for kh=5 darcy-m, total mass flow rate for Swi=0.5 gradually decreases with an increase in wellhead pressure, P_{WH}, but it quickly starts decreasing at about P_{WH}=30 bar. After the curve reaches the maximum wellhead pressure at about 37 bar, both the wellhead pressure and the flow rate start decreasing. On the other hand, the curve for Swi=0.1 shows small changes in flow rate over a wide range of wellhead pressure. Small flow rates as P_{WH} decrease in both curves may not be realized in practical situations as the flow in wellbore becomes unstable. Relationship between wellhead pressure and total flow rate represents similar curves regardless to the values of kh as shown in **Fig. 2(a)** and **(b)**. The lower kh, however, gives lower flow rate in general.

The water and steam flow rates versus wellhead pressure are illustrated in **Fig. 3(a)**, **(b)** for kh=5 darcy-m, and **Fig. 4(a)**, **(b)** for kh=3 darcy-m. The curves for water flow rate

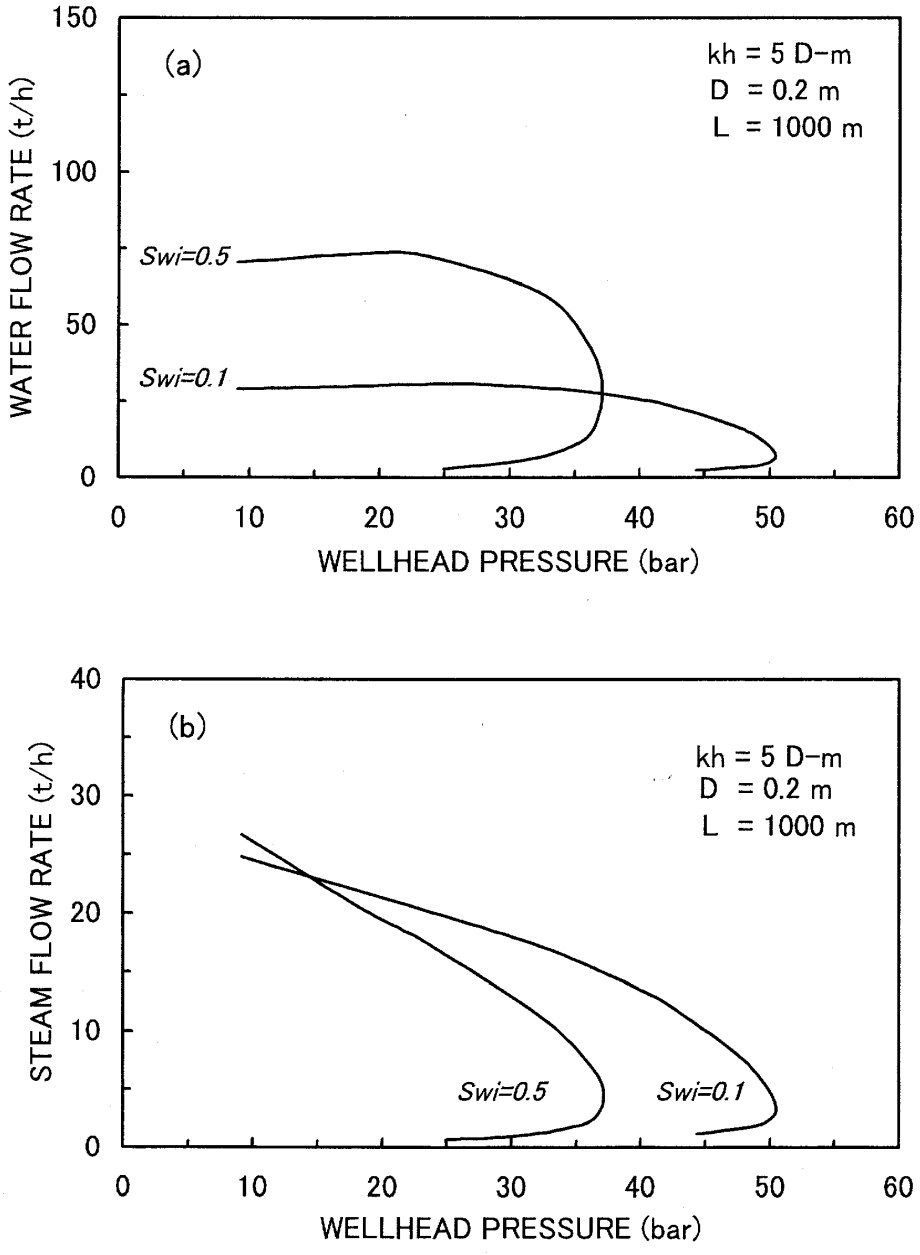

Fig. 3 Well deliverability curves of water (a) and steam (b) for different Swi (kh=5 darcy-m).

versus wellhead pressure show similar relationship as the case of the total flow rate. However, small decline in the water flow rate can be seen as P_{WH} decreases in both curves of *Swi*. On the other hand, both curves of steam flow rate show the highest values at the lowest P_{WH} in a pressure range as shown in **Fig. 3(b)** and **Fig. 4(b)**, then decreases linearly with an increase in P_{WH} up until it reaches to the maximum value. High values of steam flow rate at low P_{WH} result in a slight increase in total flow rate in low P_{WH} range as shown in **Figs. 2(a)** and **(b)** in spite of decreases in the water flow rate as P_{WH} decrease.

4.2 Behaviors of deliverability curves

Figure 2 shows that the total flow rates for lower initial water saturation, $Swi=0.1$, are always below those for higher $Swi=0.5$ for relatively high total flow rates. In other words, as the flow rate increases the deliverability curve for $Swi=0.1$ intersects that for $Swi=0.5$,

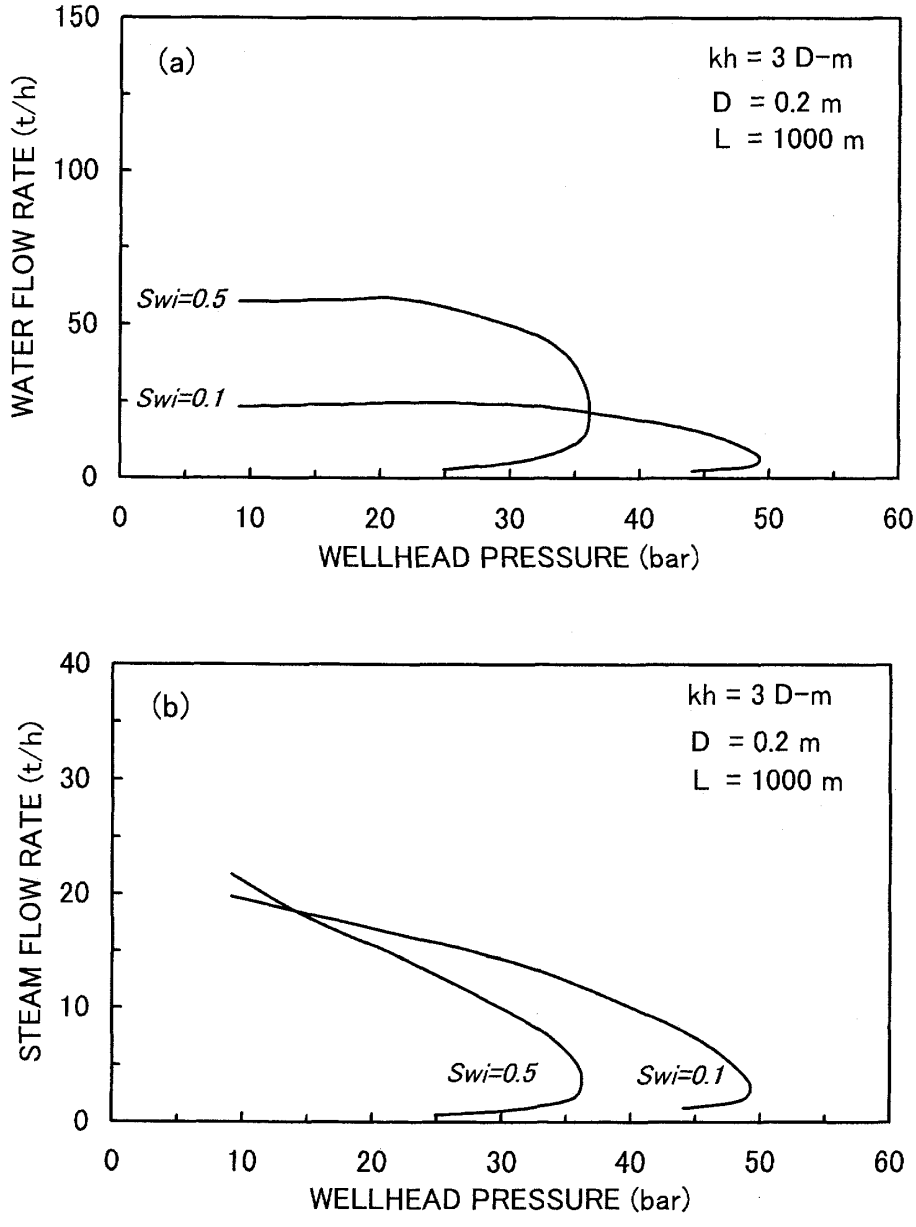

Fig. 4 Well deliverability curves of water (a) and steam (b) for different *Swi* ($kh=3$ darcy-m).

then it goes further below it. To explain this situation, the relationships between feed zone pressures and total flow rates for different *Swi* are examined. All curves in **Fig. 5** indicate that the decrease in the feed zone pressures, *Pwb*, results in the increase in the total flow rate regardless of *Swi*. At a given *Pwb*, the smaller the *Swi* is, the less total flow rate will be. It is obvious from Eq. (9) that the total flow rate depends primarily on two dependent variables: feed zone pressure (*Pwb*) and integrated total kinematic viscosity (ν_t). Distributions of ν_t in the vicinity of well for different values of *Swi* are presented in **Fig. 6**. It can be seen that the ν_t of *Swi*=0.1 shows higher values compared with that of *Swi*=0.5 at a given mass flow rate (50 t/h). Mass flow rate from the reservoir into the wellbore depends on permeability thickness, total kinematic viscosity and pressure gradient at wellbore radius as indicated by Eq. (9). This is the reason why the decrease in *Swi* causes the decrease in the total flow rate at a given feed zone pressure as shown in **Fig. 5**.

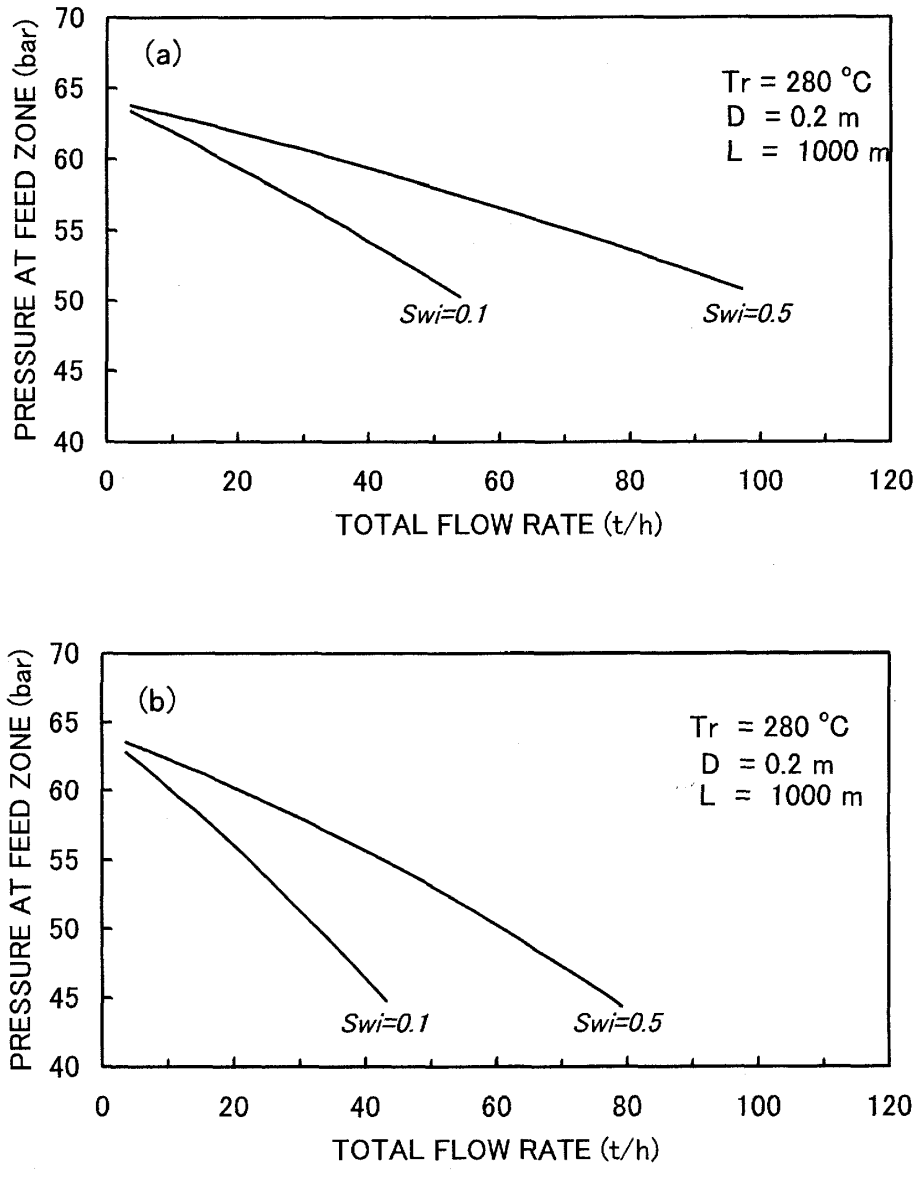

Fig. 5 Pressure at feed zone vs total flow rate: (a) *kh*=5 darcy-m, (b) *kh*=3 darcy-m.

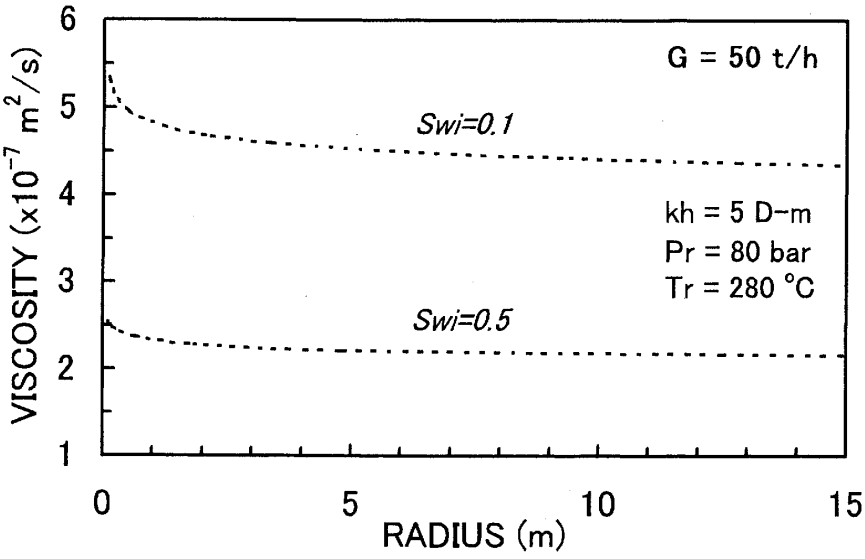

Fig. 6 Kinematic viscosity distributions in the reservoir for different *Swi*.

4.3 Characteristics of flowing pressures in wellbore

The pressure profiles in wellbores are presented in **Fig. 7** for two different wellhead pressures of P_{WH}, 35.1 bar and 10.1 bar under the conditions of two different values of initial water saturations; Swi= 0.5 (●, ■) and 0.1 (○, □). The circles represent the high wellhead

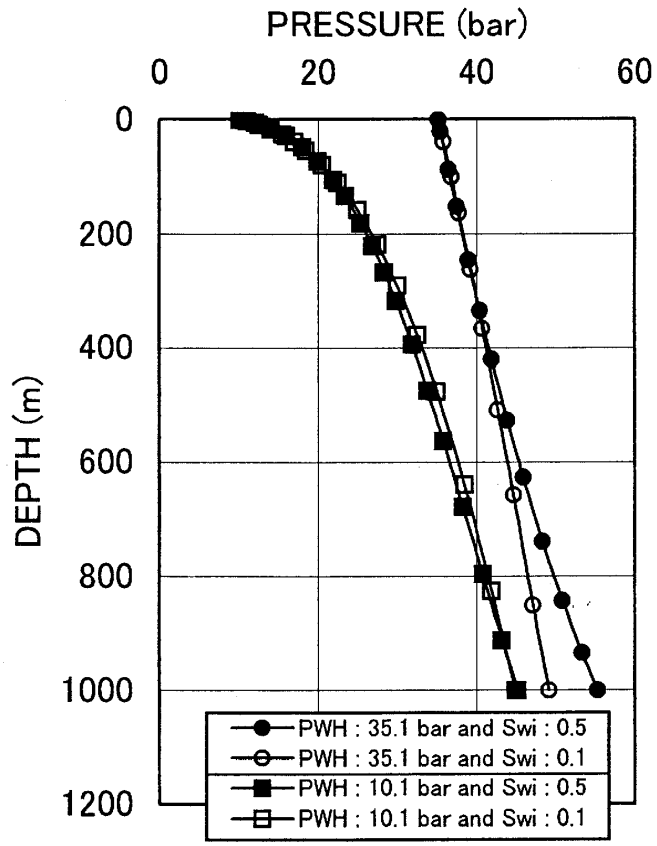

Fig. 7 Pressure profiles for different P_{WH} and *Swi*.

Table 2 Calculated results on well parameters.

Wellhead Pressure (bar)	Feedzone Pressure (bar)	Pressure Drop		Initial Water Saturation (-)	Mass Flow Rate (t/h)
		Wellbore (bar)	Reservoir (bar)		
35.1	55.3	20.2	8.65	0.5	42
35.1	49.1	14.0	14.9	0.1	35
10.1	45.2	35.1	18.9	0.5	80
10.1	45.0	34.8	19.1	0.1	43

pressure whereas the squares represent the low wellhead pressure. The permeability thickness of 3 darcy-m is used. The main features of the pressure profiles due to the differences in P_{WH} can be found at the uppermost part of the wells. For the case of high P_{WH} the pressure profile decreases linearly up to the wellhead, while the case for low P_{WH} the pressure drops markedly near wellhead. Simulated results are summarized in **Table 2**.

In the case of high P_{WH} (●, ○) in **Fig. 7**, the effects of *Swi* are significant on the pressure profiles. The decrease in *Swi* from 0.5 to 0.1 gives remarkable change in well bottom pressure from 55.3 bar to 49.1 bar. On the other hand, for the low P_{WH} case the changes in *Swi* from 0.5 to 0.1 does not give any differences in pressure profiles. The pressure profiles are linear from the bottom up to the depth of about 500 m and rapidly decrease as they approach to the wellhead. In terms of total mass flow rates, the decrease in *Swi* from 0.5 to 0.1 leads to decrease in mass flow rates by 15% for P_{WH}=35.1 bar and 52% for P_{WH}=10.1 bar.

Figure 8 (a), **(b)**, **(c)** and **(d)** show the components of pressure drop versus depth in a wellbore (potential, acceleration and friction) at given P_{WH} and *Swi*. In general, the potential component decreases as the fluid approaches the wellhead while the other two components increase. In the case of high P_{WH} and *Swi* (35.1 and 0.5 respectively), as shown in **Fig. 8 (a)**, the pressure drop is dominated by a potential component followed by a friction and finally an acceleration component. In the case of high P_{WH} (=35.1) and low *Swi* (=0.1), as shown in **Fig. 8 (b)**, the potential component decreases significantly as the fluid approaches the wellhead while the friction component increases markedly. The increase in the acceleration component is very small and has a negligible value when fluid flows upwards. An important feature for the high P_{WH} case regardless of *Swi* is the change in the pressure drop for each component almost linearly decreases from the bottom to the top. This is the reason why the pressure profiles in the wellbore for high P_{WH} also linearly decrease as fluid flows upward.

Different features are observed in **Fig. 8 (c)** and **(d)**. For the low P_{WH} case (=10.1 bar), the potential component decreases as the fluid flows upwards while the acceleration and friction components increase. Regardless to *Swi*, the potential component reaches negligible small at wellhead. The decrease rate in the pressure drop due to potential component with depth is larger for high *Swi* (=0.5). The increase rate for friction component to the depth is also larger for high *Swi* (=0.5). In the case of low P_{WH} case (=10.1 bar), the acceleration component increases markedly when fluid approaches the wellhead. The larger increase rate is observed for high *Swi* (=0.5). This acceleration pressure drop profile at the uppermost part of the well may cause the pressure profiles to decrease sharply as the fluid approaches the wellhead. This is because the velocity increases rapidly as it approaches the wellhead.

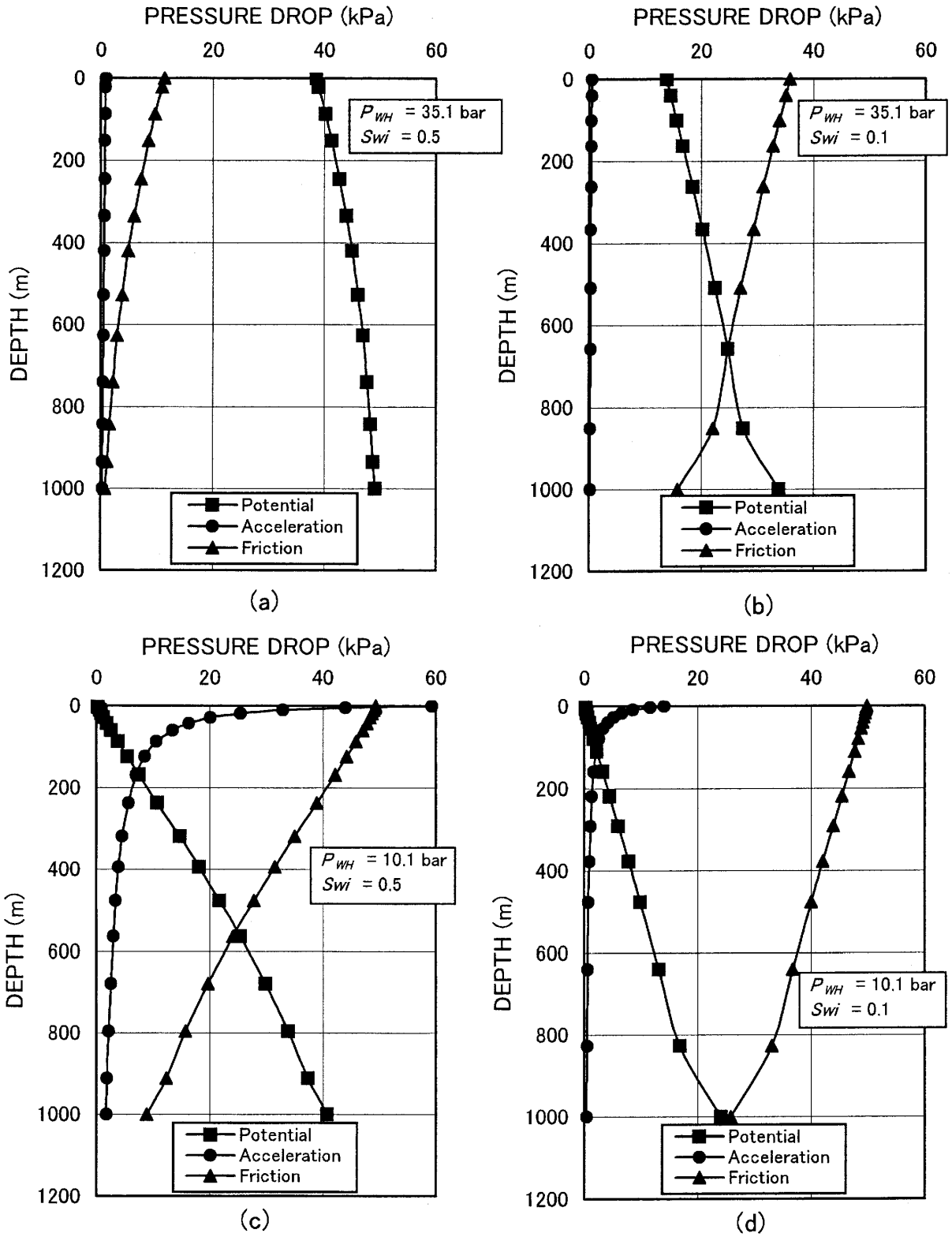

Fig. 8 Pressure drops components at depth for different P_{WH} and Swi: (a) P_{HW}=35.1 bar, Swi=0.5, (b) P_{WH}=35.1 bar, Swi=0.1, (c) P_{HW}=10.1 bar, Swi=0.5, and (d) P_{HW}=10.1 bar, Swi=0.1.

5. Conclusions

From the above analyses, the following conclusions have been drawn:

1. In the analysis of well characteristics for two-phase reservoir, the initial water saturation in the reservoir plays an important role besides the reservoir pressure and temperature.
2. The smaller initial water saturation results in the less total flow rate at a given wellhead pressure. However, the decrease in the initial water saturation causes an increase in the maximum discharge pressure.
3. The total flow rate stabilizes as the wellhead pressure becomes smaller whereas the steam flow rate linearly increases.
4. The total flow rate at the feed zone increases in a non-linear manner as the feed zone pressure decreases. At a given feed zone pressure, lower initial water saturations results in higher mass flow rates.
5. At low wellhead pressures, the pressure profiles at the uppermost part of the wellbore are controlled by the pressure drop due to acceleration.

Acknowledgements

The first author gratefully acknowledges the financial support of the Ministry of Education, Culture, Sports, Science and Technology, Government of Japan in the form of scholarship, so the first author gets a chance to attend the master and doctor course at Dept. of Earth Resources Engineering, Kyushu University.

References

1) Bjornsson, G. and Bodvarsson, G. S. (1987) A Multi-Feedzone Wellbore Simulator. Geothermal Resources Council Trans., Vol.11, 503-507.
2) Hadgu, T. and Freeston, D. H. (1990) A Multipurpose Wellbore Simulator. Geothermal Resources Council Trans, Vol.14, 1279-1286.
3) Takahashi, M. (1999) Development of a Flow Simulator (WELCARD-V) Considering Inflow Performance and Wellbore Performance of Geothermal Well. Journal of the Geothermal Research Society of Japan, Vol.21, 341-352.
4) Hadgu, T. and Zimmerman, R. W. and Bodvarsson, G. S. (1995) Coupled Reservoir-Wellbore Simulation of Geothermal Reservoir Behavior. Geothermics, Vol.24, 145-166.
5) Gudmundsson, J.S. (1984) Discharge Analysis Method for Two-Phase Geothermal Wells. Geothermal Resources Council, Vol.8, 295-299.
6) Brennand, A.W. and Watson, A. (1987) Use of ESDU Compilation of Two-Phase Flow Correlations for The Prediction of Well Discharge Characteristics. Proceedings of 9th NZ Geothermal Workshop, 65-68.
7) Garg, S. K., Combs, J. and Livesay, B. J. (2000) Optimizing Casing Designs of Slim Holes for Maximum Discharge of Geothermal Fluids from Liquid Feedzones. Proceedings World Geothermal Congress, Kyushu-Tohoku, Japan May 28 — June 10, 1145-1150.
8) Guiterrez, A. G., Paredes, G. E. and Ramirez, I. H. (2001) Study on The Flow Production Characteristics of Deep Geothermal Wells. Geothermics, Vol.31, 141-167.
9) Garg, S.K. and Combs, J. (1995) Production/Injection Characteristics of Slim Holes and Large-Diameter Wells at The Sumikawa Geothermal Field, Japan. Proceedings Twenti-eth Workshop on Geothermal Reservoir Engineering, Stanford University, Stanford,

California, 31-39.
10) Itoi, R., Kakihara, Y., Fukuda, M. and Koga, A. (1988) Numerical Simulation of Well Characteristics Coupled with Radial Flow in A Geothermal Reservoir. International Symposium on Geothermal Energy, Kumamoto and Beppu, Japan, 201-204.
11) Grant, M.A., Donaldson, I.G. and Bixley, P.F. (1982) Geothermal Reservoir Engineering. Academic Press, 369p.
12) Orkiszewski, J. (1967) Predicting Two-Phase Pressure Drops in Vertical Pipe. Journal of Petroleum Technology, 829-838.
13) Lindeburg, M.R. (1992) Engineering — Training Reference Manual 8th Edition. Professional Publications, Inc,.
14) Ito, T. (1993) PROPATH: A program package for thermodynamical properties of fluids, version 8.1.